Imaging of thickness and compositional fluctuations in InGaN/GaN quantum wells by scanning capacitance microscopy

X. Zhou and E. T. Yu[a)]
Department of Electrical and Computer Engineering, University of California, San Diego, La Jolla, California 92093-0407

D. I. Florescu, J. C. Ramer, D. S. Lee, S. M. Ting, and E. A. Armour
Veeco TurboDisc Operations, 394 Elizabeth Avenue, Somerset, New Jersey 08873

(Received 28 March 2005; accepted 19 April 2005; published 25 July 2005)

We have used scanning capacitance microscopy (SCM) and atomic force microscopy (AFM) to characterize structural and electronic properties of $In_xGa_{1-x}N/GaN$ quantum-well structures at the nanoscale. Macroscopic capacitance-voltage measurements combined with numerical simulations indicate that either electron or hole accumulation in the quantum-well layer can be induced by application of forward or reverse bias, respectively. Under reverse bias conditions (hole accumulation), features corresponding to monolayer fluctuations in $In_xGa_{1-x}N$ quantum-well thickness are clearly evident. Under forward bias conditions (electron accumulation), samples exhibiting high luminescence efficiencies are found to contain regions of increased carrier accumulation within the quantum well, which on the basis of spatially resolved spectroscopy, bias-dependent imaging, and numerical simulations are attributed to nanoscale In-rich clusters in the quantum well. No such features are observed in samples exhibiting lower luminescence efficiencies. Together, these studies demonstrate the ability to image, and distinguish, nanoscale variations in subsurface electronic properties arising from either monolayer thickness fluctuations or compositional inhomogeneities in $In_xGa_{1-x}N/GaN$ quantum-well structures. © *2005 American Vacuum Society.* [DOI: 10.1116/1.1947799]

I. INTRODUCTION

$In_xGa_{1-x}N/GaN$ quantum-well structures are of outstanding current interest for nitride semiconductor-based visible light emitters, including both light-emitting diodes and laser diodes.[1,2] Although dramatic advances have been made in the development of such devices, the optimization of emission efficiencies, particularly over a wide range of visible wavelengths and, consequently, In composition in the quantum well, requires a detailed understanding of the local, nanoscale structure and associated electronic properties in the $In_xGa_{1-x}N/GaN$ quantum-well region.[3–7] In particular, factors such as the thickness of the quantum-well layer, which influences the degree of wave-function overlap between electrons and holes and consequently the recombination dynamics and efficiency, and the possible presence of compositional inhomogeneities such as clustering or phase separation in the $In_xGa_{1-x}N$ layer, which are believed to play a significant role in the attainment of high emission efficiencies in certain structures, can dramatically influence emission properties. Direct characterization at the nanoscale of these and related aspects of quantum-well structure, however, remains a substantial experimental challenge.

In this paper, we describe studies of $In_xGa_{1-x}N/GaN$ quantum-well structures using scanning capacitance microscopy (SCM) and scanning capacitance spectroscopy (SCS) in which local, nanometer-scale electronic behavior is characterized and its origin in local structure and composition of the quantum-well layer elucidated. By obtaining SCM images at different bias voltages encompassing both forward- and reverse-bias conditions, and using numerical simulations to determine the relationship between capacitive behavior and $In_xGa_{1-x}N/GaN$ quantum-well thickness and In concentration, it is possible to detect the presence of both monolayer fluctuations in quantum-well thickness and nanoscale In-rich clusters in the $In_xGa_{1-x}N$ layer, and furthermore to distinguish between these features on the basis of their different manifestations under forward- and reverse-bias conditions. The ability to image electronic structure associated with nanometer to atomic scale structural features in subsurface quantum-well layers is particularly noteworthy given the difficulty of directly imaging subsurface electronic properties in semiconductors at these length scales. In addition, the presence of In-rich clusters is observed to correlate with an increase in optical emission efficiency, corroborating suggestions that carrier localization in such clusters contributes significantly to improved device performance in $In_xGa_{1-x}N/GaN$-based light emitters.[7]

II. EXPERIMENT

The samples employed in these studies, whose structure is shown representatively in Fig. 1, were grown by metalorganic chemical vapor deposition (MOCVD) on a *c*-plane sapphire substrate using a Veeco TurboDisc E300 GaNzilla platform. Samples consisting of a 2–3 μm *n*-GaN buffer layer with doping concentration of approximately $10^{18}/cm^3$ followed by a 3–3.5 nm undoped $In_xGa_{1-x}N$ quantum-well

a)Electronic mail: ety@ece.ucsd.edu

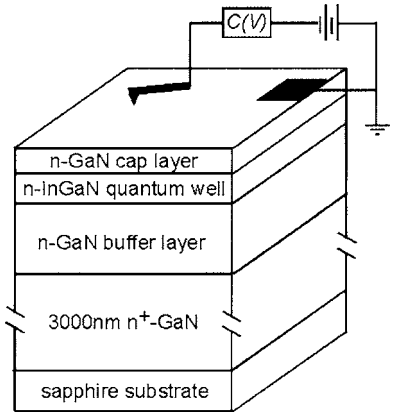

FIG. 1. (a) Schematic diagram of a representative $In_xGa_{1-x}N/GaN$ quantum-well structure showing contact and scanning probe measurement geometry.

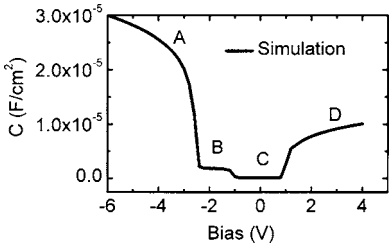

FIG. 2. Numerically simulated capacitance-voltage spectrum for a 3 nm $In_{0.30}Ga_{0.70}N/GaN$ quantum-well structure.

layer with In concentrations ranging from 15% to 30% were studied. The 30% $In_xGa_{1-x}N$ quantum well was grown at 710 °C while the 15% was grown at 760 °C. In each epitaxial layer structure, the $In_xGa_{1-x}N$ quantum-well layer was capped with 2 nm undoped GaN; the proximity of the quantum-well region to the sample surface enabled very high spatial resolution to be achieved in SCM characterization.[8] Composition and layer thicknesses were estimated from MOCVD growth conditions and verified (postgrowth) by x-ray diffraction (XRD) measurements and XRD simulation of the epitaxial layer structures. More detailed descriptions of sample preparation, growth conditions, and growth parameters have been presented elsewhere.[9]

All samples were cleaned with trichloroethylene, acetone, and methanol in an ultrasonic bath, followed by a rinse in isopropanol and then acid cleaning using $HCl:H_2O$ (1:1) prior to processing or imaging. Ohmic contacts were fabricated on all samples by deposition of 33 nm Ti/77 nm Al/33 nm Ti/88 nm Au followed by annealing at 650 °C for 3 min. Scanning capacitance microscopy and spectroscopy were performed in a Digital Instruments/Veeco Nanoscope IIIa Dimension 3100s scanning probe microscopy system using Co/Cr-coated tips with a nominal tip radius of 25–50 nm. To assist in the interpretation of scanning capacitance data, numerical simulations of capacitance-voltage spectra were performed using a one-dimensional Poisson-Schrödinger solver[10] with band offsets and polarization charge densities at the $In_xGa_{1-x}N/GaN$ interfaces derived from experimentally measured values.[11]

The SCM and SCS techniques employed here have been described in detail elsewhere.[12,13] In brief, a voltage signal with dc and low-frequency ac (5–100 kHz) components is applied between a conductive probe tip and the sample, which are connected to a capacitance sensor through a transmission line tuned at its resonant frequency of approximately 915 MHz. The signals extracted from the measurement are proportional to the magnitude of dC/dV. SCM images are obtained by scanning the probe tip and measuring the signal as a function of tip position. Spectroscopic data are obtained by either (i) measuring the signal while slowly sweeping the dc bias voltage with the tip held stationary in contact with the sample, or (ii) obtaining a series of SCM images at different bias voltages, and extracting the spatially resolved signal from each image to construct a collection of spatially resolved signal spectra.

III. RESULTS AND DISCUSSION

A. Numerical simulations

We have simulated the expected capacitance-voltage spectra for Schottky contacts formed to the $In_xGa_{1-x}N/GaN$ quantum-well structures studied here to determine the relationship between capacitive behavior and variations in quantum-well structure, most notably variations in quantum-well thickness and In concentration. Figure 2 shows a simulated capacitance-voltage spectrum for a 3 nm $In_{0.30}Ga_{0.70}N/GaN$ quantum-well sample; the capacitance-voltage behavior for other compositions and quantum-well thickness studied is very similar. The simulated capacitance-voltage spectrum was verified qualitatively by comparison with results of capacitance-voltage spectroscopy performed on large-area Schottky diodes; detailed quantitative comparisons were difficult due to substantial series resistances present in the Schottky diodes. Several regimes of behavior, corresponding to accumulation of different carrier types, either electrons in the $In_{0.30}Ga_{0.70}N$ quantum well or holes in the quantum well or near the GaN surface, are observed in both the simulation and macroscopic capacitance-voltage measurement. At large negative bias voltages (region A), hole accumulation near the upper $In_{0.30}Ga_{0.70}N/GaN$ interface and in the top GaN layer occurs, leading to a large capacitance. As the bias voltage is increased to values near −2 V (region B), hole accumulation occurs primarily near the lower $In_{0.30}Ga_{0.70}N/GaN$ interface, resulting in a lower capacitance. For voltages near zero bias (region C), carriers are depleted from the $In_{0.30}Ga_{0.70}N/GaN$ quantum-well structure and only a small depletion capacitance is present. Finally, for larger forward bias voltages applied to the Schottky contact (region D), a large capacitance due to electron accumulation at the upper $In_{0.30}Ga_{0.70}N/GaN$ interface and in the top GaN layer is observed. Thus, we see that numerical simulations confirmed by macroscopic capacitance-voltage measurements indicate that either electron or hole accumulation in the quantum-well layer can be induced by application of forward or reverse bias, respectively.

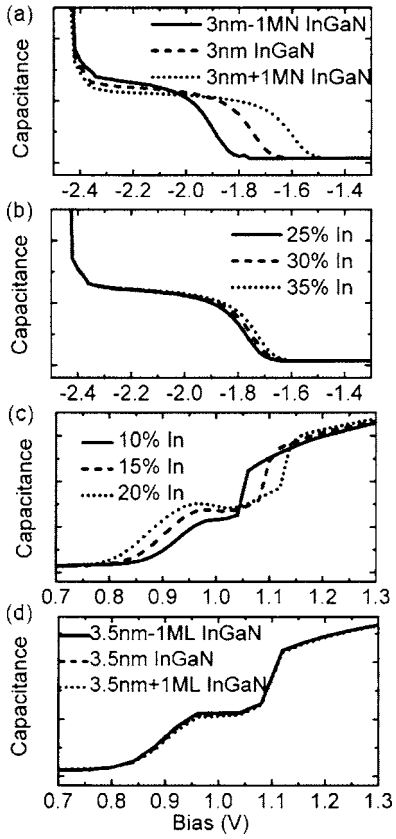

FIG. 3. Simulated capacitance-voltage spectra for (a) $In_{0.30}Ga_{0.70}N$ quantum well with thicknesses of 3 nm plus or minus one monolayer in reverse bias, (b) 3 nm $In_xGa_{1-x}N$ quantum well with 25%, 30%, and 35% In concentration in reverse bias, (c) 3.5 nm $In_xGa_{1-x}N$ quantum well with 10%, 15%, and 20% In concentration in forward bias, and (d) $In_{0.15}Ga_{0.85}N$ quantum well with thickness of 3.5 nm plus or minus one monolayer in forward bias.

To better understand how the detailed sample structure influences its electronic properties, we performed numerical simulations of capacitance-voltage spectra for structures with varying $In_xGa_{1-x}N$ quantum-well thickness and In concentration. These simulations do not include possible effects of surface and bulk trapping of carriers, which in principle, and occasionally in practice,[14] can substantially influence both macroscopic capacitance-voltage measurements and scanning capacitance microscopy and spectroscopy. However, analysis of SCM images of the samples characterized in the present studies obtained before and after localized application of bias voltage via a scanning probe tip indicate that such effects have little if any influence on SCM images and local spectroscopic measurements over the range of bias voltages employed in the studies presented here.

Results for two quantum-well structures, corresponding to the two samples for which experimental data will be presented, are shown. Figure 3(a) shows the simulated capacitance-voltage spectrum for reverse (negative) bias voltages for structures with $In_{0.30}Ga_{0.70}N$ quantum wells 3 nm plus or minus one monolayer in thickness. In the simulation, a variation in quantum-well thickness of one monolayer is seen to shift the threshold voltage for hole accumulation by ~0.3 V; similar variations in the thickness of the top GaN layer (nominally 2 nm) result in much smaller changes in this threshold voltage. Figure 3(b) shows reverse-bias capacitance-voltage spectra for structures with 3 nm $In_xGa_{1-x}N$ quantum wells with In concentrations of 25%, 30%, and 35%; it is evident from the figure that variations in In concentration lead to much smaller changes in threshold voltage for hole accumulation than do monolayer fluctuations in quantum-well thickness. Figure 3(c) shows simulated forward-bias capacitance-voltage spectra for 3.5 nm $In_xGa_{1-x}N$ quantum-well structures with In concentrations of 10%, 15%, and 20%; these simulations show that In concentration fluctuations very substantially influence capacitance-voltage spectra in this voltage range. Figure 3(d) shows forward-bias capacitance-voltage spectra for $In_{0.15}Ga_{0.85}N$ quantum-well structures with thicknesses of 3.5 nm plus or minus one monolayer; the influence of quantum-well thickness fluctuations on capacitance-voltage spectra in this voltage range is seen to be minimal.

The simulation results shown in Fig. 3 provide a basis for using SCM imaging to distinguish between local variations in electronic structure that arise from fluctuations in $In_xGa_{1-x}N$ quantum-well thickness and those that arise from variations in local In concentration. Specifically, we see from Figs. 3(a) and 3(b) that, under reverse-bias conditions, the capacitance-voltage spectrum for the quantum-well structure is most strongly influenced by the thickness of the $In_xGa_{1-x}N$ quantum well, and only weakly dependent on the In concentration. Thus, features in SCM imaging under reverse-bias conditions are most likely to reflect local variations in electronic structure arising from quantum-well thickness fluctuations—even at the monolayer level. We see from Figs. 3(c) and 3(d) that, under forward-bias conditions, the capacitance-voltage spectrum is most strongly influenced by variations in In concentration, and only minimally dependent on quantum-well thickness. Thus, features in SCM imaging observed under forward-bias conditions will predominantly reflect variations in electronic structure arising from local variations in In concentration rather than quantum-well thickness.

B. Monolayer quantum-well thickness fluctuations

Figure 4 shows topographic and scanning capacitance images of a 3 nm $In_{0.30}Ga_{0.70}N/GaN$ quantum-well sample structure for both forward bias and reverse bias. Monolayer steps approximately 2.5–3 Å in height, indicative of step-flow growth, are clearly visible in the topographic image, as are pinned step edges terminated by screw-component dislocations.[15] With the probe tip under forward-bias conditions relative to the sample, as shown in Fig. 4(b) for a representative bias value of +2 V, little contrast is evident. Under reverse-bias conditions, however, pronounced contrast in SCM imaging is evident. At −2.25 V, small undulations are visible in SCM imaging, as shown in Fig. 4(c); and at −2.5 V these variations in contrast are much more evident with additional structural detail becoming clearly visible, as shown in Fig. 4(d).

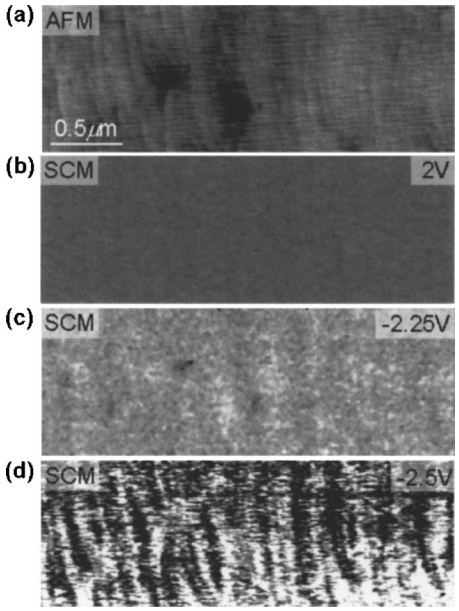

FIG. 4. (a) Topographic image and (b–d) scanning capacitance images of the 3 nm $In_{0.30}Ga_{0.70}N/GaN$ quantum-well structure. Features corresponding to monolayer fluctuations in $In_{0.30}Ga_{0.70}N$ quantum-well thickness are apparent under reverse bias, but absent, as expected, under forward bias.

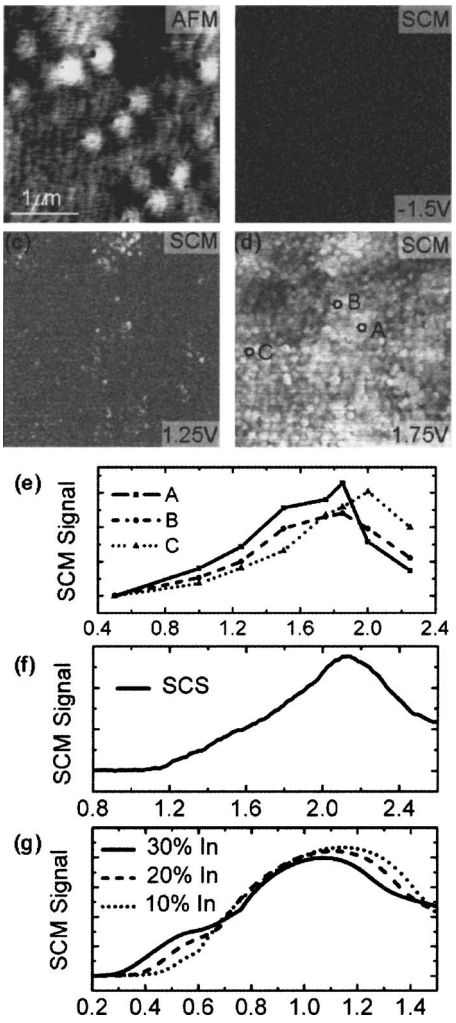

FIG. 5. (a) Topographic image and (b–d) scanning capacitance images of the 3.5 nm $In_{0.15}Ga_{0.85}N/GaN$ quantum-well structure. Bias voltages are indicated for each SCM image. Data scale is 2 V for (b), (c), and 4 V for (d). (e) SCM signal spectra extracted from images obtained at different bias voltages at points labeled A, B, and C in (d). (f) Representative single SCM signal spectrum. (g) Computed capacitance-voltage spectra for $In_xGa_{1-x}N$ quantum-well structures with In concentrations of 10%, 20%, and 30%.

On the basis of the numerical simulations described in Sec. III A the contrast in these images can clearly be interpreted as arising from local variations in hole accumulation, induced by the negative bias applied to the tip, in or near the $In_{0.30}Ga_{0.70}N$ quantum well. The differences in voltages at which various contrast features occur experimentally and in numerical simulations are due primarily to the effects of finite tip size, tip shape, and series resistance in the sample, as analyzed in detail in prior studies.[16] The observation of strong SCM image contrast under reverse-bias conditions combined with the lack of such contrast in forward-bias SCM imaging strongly indicates that the features observed in Figs. 4(c) and 4(d) arise from local variations in thickness of the $In_{0.30}Ga_{0.70}N$ quantum well, as even monolayer variations in quantum-well thickness lead to substantial changes in the reverse-bias capacitance-voltage spectra. Indeed, a more detailed analysis of reverse-bias SCM and SCS data obtained for this sample structure, presented elsewhere,[8] offers further evidence that the SCM image features seen in Figs. 4(c) and 4(d) arise from monolayer fluctuations in the thickness of the $In_{0.30}Ga_{0.70}N$ quantum-well layer.

C. Nanoscale In clustering

Figure 5 shows representative 3 μm $\times$ 3 μm topographic and scanning capacitance images of a 3.5 nm $In_{0.15}Ga_{0.85}N/GaN$ quantum-well sample structure for a series of tip bias voltages including both reverse bias and forward bias conditions. With the probe tip under reverse bias relative to the sample, little contrast is evident in the SCM image, as shown in Fig. 5(b). Under forward bias, however, we see in Fig. 5(c) that at +1.25 V, isolated, approximately circular areas 30–50 nm in radius with increased SCM signal levels are observed, and at 1.75 V these and additional regions of increased SCM signal level are much more evident, as seen in Fig. 5(d). The characteristic radius of the features visible at 1.25 V increases to 35–55 nm at 1.75 V, suggesting a corresponding expansion of the area within which electron accumulation occurs. The actual size of these features is, of course, considerably smaller than the size observed in the image due to tip convolution and sample depletion effects. Very approximately, the observed radius of a given feature will be the sum of the probe tip radius (typically 25–50 nm), the depletion depth within the sample (a few nm in our studies due to the proximity of the quantum well to the surface), and the actual feature size, which based on this approach we estimate to be 25 nm or smaller. The density of these features is $\sim 2 \times 10^9$ cm^{-2} at 1.25 V bias and $\sim 8 \times 10^9$ cm^{-2} at 1.75 V.

The observation of these features under forward-bias conditions, but not under reverse bias, combined with the results of numerical simulations as discussed in Sec. III A, indicates that the features observed in Figs. 5(c) and 5(d) arise from local variations in In concentration within the quantum well. Spatially resolved scanning capacitance spectroscopy combined with numerical simulations provides further insight into the origins of the SCM contrast features. Figure 5(e) shows spatially resolved scanning capacitance spectra for three locations marked within the SCM image, constructed by extracting SCM signal levels from a series of images obtained at different bias voltages. Points A and B correspond to circular regions in which increased SCM signal levels are observed at bias voltages of 1.25–1.75 V, and point C to a region of approximately average signal level at these voltages. A single representative scanning capacitance spectrum measured directly for this sample is shown in Fig. 5(f); the similarity of this spectrum to the spectra extracted from image data and shown in Fig. 5(e) confirms the validity of the latter.

To interpret the variations in the SCM signal spectra that are evident in Fig. 5(e), we employ numerical simulations of capacitance-voltage spectra, from which the expected SCM signal spectrum is computed.[16] Figure 5(g) shows scanning capacitance spectra computed in this manner for In concentrations in the quantum well of 10%, 20%, and 30%. A comparison of the experimental SCM signal spectra in Fig. 5(e) with the computed spectra indicates that the circular areas exhibiting increased signal level in the SCM images correspond to localized regions of In-rich material in the quantum well. Specifically, a comparison of the spectra at points A and B with that at point C reveals that for points A and B, a higher signal level is observed at relatively low bias voltages, while a lower signal level is measured at higher bias voltages (approximately +2.0 V and above). As is evident in the simulated SCM signal spectra, this behavior is consistent with the presence of increased local In concentration at points A and B relative to that at point C. Figure 2(d) indicates that local variations in thickness of an $In_{0.15}Ga_{0.85}N$ quantum-well layer lead to only very minor changes in the capacitance spectra at these bias voltages, and therefore that the observed variations in SCM signal spectra are unlikely to arise from quantum-well thickness variations.

We occasionally observe contrast similar to that exhibited in the In-rich regions in the immediate vicinity of threading dislocations, such as those visible as dark pits in Fig. 5(a). Because threading dislocations in nitride semiconductor material frequently contain deep acceptor states,[17–19] one might anticipate that at positive tip bias voltages these states would be negatively charged, resulting in an increase in electron potential energy and localized depletion of electrons in the vicinity of the dislocation line. However, computational studies of GaN Schottky barriers in the vicinity of charged dislocations have shown that pinning of the Fermi level can suppress the increase in potential energy very near the GaN surface,[20] so that the quantum-well carrier concentration in our samples is most likely relatively unaffected by proximity to a charged dislocation line.

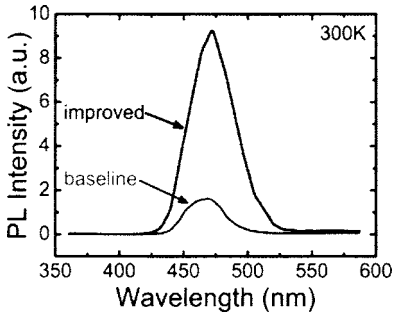

FIG. 6. Room-temperature photoluminescence spectra for nominally identical 3.5 nm $In_{0.15}Ga_{0.85}N/GaN$ quantum-well structures grown under conditions leading to formation of In-rich clusters ("improved") and under conditions for which such clusters are absent ("baseline").

We have also found that the observation of In clustering in the $In_xGa_{1-x}N$ quantum-well region by SCM is correlated with dramatically increased photoluminescence efficiency compared to that measured for nominally identical samples grown under conditions for which formation of In-rich regions was not observed. Figure 6 shows room-temperature photoluminescence spectra for two nominally identical 3.5 nm $In_{0.15}Ga_{0.85}N/GaN$ quantum-well structures, except that the structure labeled "baseline" was grown under conditions for which In clustering is not observed in our SCM measurements, while the structure labeled "improved" was grown under conditions leading to the formation of In-rich clusters as observed in our SCM studies described above. The latter structure exhibits a much higher luminescence efficiency, presumably due to enhanced recombination of excitons localized at potential minima created by nanoscale In-rich regions. The increased linewidth of the photoluminescence spectrum for the sample containing In-rich clusters compared with the baseline sample is most likely a consequence of inhomogeneous broadening arising from the presence of In-rich clusters with a range of compositions.

IV. CONCLUSIONS

In summary, we have used scanning capacitance microscopy and spectroscopy to characterize local electronic structure in two $In_xGa_{1-x}N/GaN$ quantum-well structures grown by MOCVD. On the basis of macroscopic capacitance-voltage measurements combined with numerical simulations, we see that either electron or hole accumulation can occur in the *n*-type quantum-well region. Furthermore, the dependence of carrier accumulation behavior, and consequently capacitance, on local variations in quantum-well layer thickness and In concentration differs substantially under forward- and reverse-bias conditions. These differences provide the basis for a methodology allowing features in local electronic structure arising from nanoscale variations in quantum-well thickness to be distinguished from those arising from variations in In concentration. This methodology is

illustrated in studies of monolayer thickness fluctuations in a 3 nm $In_{0.30}Ga_{0.70}N/GaN$ quantum-well structure, and of nanoscale In clustering in a 3.5 nm $In_{0.15}Ga_{0.85}N/GaN$ quantum-well structure. In the latter structure, the presence of In-rich clusters is further correlated with an improvement in photoluminescence efficiency, thereby offering a direct link in these structures between the presence of In-rich clusters and improved light emission characteristics.

ACKNOWLEDGMENTS

Part of this work was supported by the National Science Foundation (Grant Nos. DMR-0072912 and DMR-0405851).

[1]S. Nakamura and G. Fasol, *The Blue Laser Diode* (Springer, Berlin, 1997).
[2]Shuji Nakamura, Masayuki Senoh, Shin-ichi Nagahama, Naruhito Iwasa, Takao Yamada, Toshio Matsushita, Hiroyuki Kiyoku, Yasunobu Sugimoto, Tokuya Kozaki, Hitoshi Umemoto, Masahiko Sano, and Kazuyuki Chocho, Appl. Phys. Lett. **72**, 211 (1998).
[3]J. L. Sanchez-Rojas, J. A. Garrido, and E. Munoz, Phys. Rev. B **61**, 2773 (2000).
[4]F. A. Ponce, D. Cherns, W. Goetz, and R. S. Kern, Mater. Res. Soc. Symp. Proc. **482**, 453 (1998).
[5]N. Duxbury, U. Bangert, P. Dawson, E. J. Thrush, W. Van der Stricht, K. Jacobs, and I. Moerman, Appl. Phys. Lett. **76**, 1600 (2000).
[6]M. Benamara, Z. Liliental-Weber, W. Swider, J. Washburn, R. D. Dupuis, P. A. Grudowski, C. J. Eiting, J. W. Yang, and M. A. Khan, Mater. Res. Soc. Symp. Proc. **572**, 357 (1999).
[7]S. Chichibu, T. Azuhata, T. Sota, and S. Nakamura, Appl. Phys. Lett. **69**, 4188 (1996).
[8]X. Zhou, E. T. Yu, D. Florescu, J. C. Ramer, D. S. Lee, and E. A. Armour, Appl. Phys. Lett. **85**, 407 (2004).
[9]D. Lu, D. I. Florescu, J. C. Ramer, D. S. Lee, V. N. Merai, A. Parekh, and E. A. Armour, Phys. Status Solidi A **202**, 795 (2005).
[10]G. L. Snider, computer program 1D Poisson/Schrödinger: A band diagram calculator, University of Notre Dame, Notre Dame, IN, 1995.
[11]H. Zhang, E. J. Miller, E. T. Yu, C. Poblenz, and J. S. Speck, Appl. Phys. Lett. **84**, 4644 (2004).
[12]K. V. Smith, E. T. Yu, J. M. Redwing, and K. S. Boutros, Appl. Phys. Lett. **75**, 2250 (1999).
[13]D. M. Schaadt, E. J. Miller, E. T. Yu, and J. M. Redwing, Appl. Phys. Lett. **78**, 88 (2001).
[14]K. V. Smith, X. Z. Dang, E. T. Yu, and J. M. Redwing, J. Vac. Sci. Technol. B **18**, 2304 (2000).
[15]B. Heying, E. J. Tarsa, C. R. Elsass, P. Fini, S. P. DenBaars, and J. S. Speck, Appl. Phys. Lett. **85**, 6470 (1999).
[16]D. M. Schaadt and E. T. Yu, J. Vac. Sci. Technol. B **20**, 1671 (2002).
[17]A. F. Wright and U. Grossner, Appl. Phys. Lett. **73**, 2751 (1998).
[18]J. Elsner, R. Jones, M. I. Heggie, P. K. Stitch, M. Haugk, Th. Frauenheim, S. Öberg, and P. R. Briddon, Phys. Rev. B **58**, 12571 (1998).
[19]B. S. Simpkins, E. T. Yu, P. Waltereit, and J. S. Speck, J. Appl. Phys. **94**, 1448 (2003).
[20]C. Tivarus, Y. Ding, and J. P. Pelz, J. Appl. Phys. **92**, 6010 (2002).